

Document downloaded from:

<http://hdl.handle.net/10251/183586>

This paper must be cited as:

Magureanu, M.; Mandache, NB.; Rizescu, C.; Bucur, C.; Cojocaru, B.; Man, IC.; Primo Arnau, AM.... (2021). Engineering hydrogenation active sites on graphene oxide and N-doped graphene by plasma treatment. *Applied Catalysis B Environmental*. 287:1-11. <https://doi.org/10.1016/j.apcatb.2021.119962>



The final publication is available at

<https://doi.org/10.1016/j.apcatb.2021.119962>

Copyright Elsevier

Additional Information

Engineering hydrogenation active sites on graphene oxide and N-doped graphene by plasma treatment

Monica Magureanu¹, N.B. Mandache¹, C. Rizescu², Cristina Bucur³, Bogdan Cojocaru², Isabela C. Man⁴, Ana Primo,⁵ Vasile I. Parvulescu², Hermenegildo Garcia⁵

¹ Department of Plasma Physics and Nuclear Fusion, National Institute for Lasers, Plasma and Radiation Physics, Atomistilor Str. 409, 077125 Magurele, Romania

monica.magureanu@inflpr.ro

² University of Bucharest, Department of Organic Chemistry, Biochemistry and Catalysis, Blv. Regina Elisabeta nr.4-12, Sector 3, 030016 Bucharest, Romania,

vasile.parvulescu@chimie.unibuc.ro

³National Institute of Materials Physics, Department of Surfaces and Interfaces, Atomistilor 405 A, 077125 Magurele, Ilfov, Romania

⁴ Center of Organic Chemistry “C.D. Nenitescu” of Romanian Academy, Bucharest, Romania

⁵ Instituto Universitario de Tecnología Química, Consejo Superior de Investigaciones Científicas-Universitat Politècnica de Valencia, Universitat Politècnica de Valencia, Av. De los Naranjos s/n, 46022 Valencia, Spain, hgarcia@qim.upv.es

Abstract

Graphene oxide (GO) and N-doped graphene [(N)G] graphenes were submitted to H₂ glow discharge under different discharge regimes, in both the negative glow and positive column plasma regions. The resulted catalysts were fully characterized using several techniques such as Raman, DRIFT and XPS spectroscopy, powder X-ray diffraction, H₂ pulse chemisorption and H₂-, CO₂- and NH₃-TPD experiments. Density functional theory calculations were performed taking a slab model of graphene sheet with an optimized C-C bond length (1.426 Å) and a 16 Å vacuum layer between sheets. An overview of these characterizations showed that the O/C atomic ratio of GO is influenced by the plasma regime, indicating the occurrence of O removal, as also predicted by DFT calculations. In the case of (N)G, the plasma treatment also removes pyridinic N with an increase of the C/N ratio. The efficiency of the plasma modification has been checked through catalytic tests in hydroisomerization of 1-octene and hydrogenation of α -methyl-styrene. Contrarily to classical thermal activation requiring high temperatures, the generation of the defects by treating with plasma occurs at voltages in the range of 2-5 kV. In consequence, the hydrogenation and isomerization of alkenes resulted with high yields and good selectivities. Graphene prepared from sodium alginate from brown algae was considered as reference in these investigations.

Keywords: Graphene oxide as catalyst; N-doped graphene as catalyst; hydrogen plasma activation of graphenes; 1-octene hydroisomerization; α -methyl-styrene hydrogenation

Introduction

There is much current interest in developing metal-free catalysts that can relieve at medium term the large dependency of heterogeneous catalysis on critical and precious metals [1, 2]. Catalysts based on carbons are sustainable when they can be derived from biomass that is a renewable resource [3-6]. As an example, chitin is the universal component of the exoskeleton of insects and Crustacea and it can be used to obtain N-doped graphene [7]. N-doped graphene has been found to be a metal-free catalyst for the aerobic oxidation of benzylic hydrocarbons [8], oxidation of CO [9] and glucose [10], and CO₂ reduction [11] among other reactions [12]. It has been proposed that carbon vacancies, heteroatoms, edges and other defects can act as catalytic sites [13]. Similarly, graphene oxide (GO) also exhibits general catalytic activity in aerobic oxidations [14].

Defects are commonly formed during the synthesis of graphenes, but they can also be generated by post-synthetic treatments [15, 16]. In this context, plasma treatment having a shallow penetration depth in solids appears to be very appropriate technique for functionalization and defect engineering in 2D materials, particularly defective graphenes and GO, to enhance their activity as catalysts [17]. Thus, early in 2009 Elias et al.[18] recommended plasma as a method for generation of defects, patterning and tailoring the surface properties of graphenes. Further studies indicated the utility of this technique to tailor surface wettability and electrical conductivity and suggested a reasonable mechanism through which these transformations occur [19, 20].

However, in spite of the proven ability of plasma to generate defects and alter properties of graphenes and the current interest of defective graphenes as metal-free catalysts, there is a scarcity of studies addressing systematically how the power and operating conditions of plasma treatment enhance the catalytic activity on different graphene types

[15]. The aim of the present study is to provide an in-depth investigation of the changes on the catalytic activity produced at two different glow discharge regimes on GO and N-doped graphene [(N)G], showing that the catalytic activity of GO and (N)G depends on the regime of plasma activation.

Previous reports have shown that H₂ plasma treatment of GO generates carbon vacancies which increase its catalytic activity as hydrogenation catalyst [22]. Product selectivity in 1-octene hydrogenation, showing also skeletal isomerization, indicated that the H₂ plasma treatment can produce additional hydrogenating and acid sites rendering a bifunctional GO catalyst. Such catalysts behave similar to noble metals supported on acid supports [22]. Hydroisomerization of 1-alkenes has been reported on bifunctional catalysts containing metal nanoparticles as hydrogenation sites deposited on basic supports like hydrotalcites or SBA-15 intercalated Mg-Al hydrotalcite [23, 24] or acid supports such as SAPO [25-27]. Skeletal hydroisomerisation of 1-octene is also possible by medium strength acid catalysts [28-32].

Besides plasma treatment of GO, defects acting as catalytic centers were also created on highly oriented pyrolytic graphite surface by plasma that broke the intrinsic sp²-hybridization of graphite, inducing surface charge localized onto defective active sites and enhancing its intrinsic electrocatalytic activity [33]. Doping of graphene by nitrogen plasma produces the grafting of at least three different N types with bonding configurations corresponding to quaternary (or graphitic), pyridinic, and pyrrolic N. Among these, pyridinic and pyrrolic N atoms change the basic properties of graphene, these types of N atoms serving as electron donor sites [34-36]. In this context, the treatment of N-doped graphenes by H₂ plasma should also produce changes in the relative distribution of N atoms among the various

types and, consequently, the plasma treatment may serve as a tool to control the population of N active sites for different reactions.

Continuing with this line of research, the present study selected GO and (N)G graphene and obtained activity data showing that the H₂ plasma regime determines in both cases their catalytic performance. 1-Octene hydroisomerization has been chosen as a test reaction to evaluate the evolution of the hydrogenation and acid-basic sites as a function of the plasma treatment.

Experimental

Catalyst preparation

Graphene was prepared from the sodium salt of alginic acid from brown algae (Sigma) that was pyrolyzed in the argon atmosphere using the following oven programme: 200 °C during 2 h for annealing and then heating at 10 °C min⁻¹ up to 900 °C for 6 h. The multilayer G powder was sonicated at 700 W during 1 h to obtain the dispersed G in the reaction mixture. GO was prepared from commercial graphite by Hummers-Offeman oxidation with KMnO₄ in concentrated KNO₃ and H₂SO₄, as reported. (N)G was obtained by pyrolysis of chitosan powder at 900 °C in an electrical oven under Ar and subsequent exfoliation in water of the carbon residue by ultrasounds.

Plasma treatment

The graphene samples were submitted to hydrogen plasma treatment. The plasma was generated in a cylindrical reactor (Φ 65 mm), containing a planar anode (Φ 40 mm) and a cylindrical hollow cathode (Φ 25 mm), placed on the axis of the tube.

After outgassing the plasma reactor at 3×10^{-3} mbar, the reaction chamber with continuously flushed with a hydrogen flow, adjusting the operating pressure at the required value from 0.2 mbar (corresponding to a H_2 flow rate of 10 mL min^{-1}) to 4 mbar (H_2 flow rate of 62 mL min^{-1}). The internal electrode was connected to the Earth, while cylindrical electrode was submitted to a constant voltage in the range of 2-5 kV. Depending on the applied voltage and treatment pressure, various plasma regimes can be obtained. The graphene samples were treated either in the negative light or in the positive column plasma regions, which are described in detail in the Supplementary Information.

Optical characterization of the plasma

Optical emission spectroscopy measurements were carried out using a spectrophotometer from Princeton Instruments model IsoPlane SCT 320 with a monochromator with Schmidt-Czerny-Turner configuration. Spectra were acquired with a CCD camera from Princeton Instruments model PI MAX4-1024i-RB, cooled at $-25 \text{ }^\circ\text{C}$. The resolution of the digital spectra was 1024×1024 pixels.

Catalysts characterization

Raman spectra were acquired with a Horiba JobinYvon-Labram spectrophotometer in the range from 150 to 4000 cm^{-1} using a 488 nm laser as excitation source. Powder XRD patterns were obtained with a Shimadzu XRD-7000 diffractometer operating at 40 kV and a

current of 40 mA, employing the CuK α radiation ($\lambda = 1.5418 \text{ \AA}$,) at a scanning speed of 0.10 degrees min⁻¹ in the 10°– 90° 2 Θ range.

DRIFT analysis was carried out using a Bruker Tensor II with a Praying Mantis accessory. A mirror was used as reference.

H₂ pulse chemisorption and H₂-TPD experiments were carried out in a Micromeritics AutoChem II 2920 station. Before the experiments, fresh samples were heated to 120 °C (20 °C min⁻¹) in 30 mL \times min⁻¹ He flow. Subsequently, the samples were cooled down to room temperature also under He flow. At room temperature, pulses of 5 vol % H₂ in He were introduced until the peak areas were the same. Subsequently, thermal desorption of H₂ was carried out heating at a constant rate (10 °C min⁻¹) in a He flow till 400 °C. CO₂-TPD and NH₃-TPD measurements were carried out using the same AutoChem II 2920 station. The samples (3–5 mg) were introduced in a quartz U-shaped tube of 0.5 cm internal diameter and were submitted to a He flow (Purity 5.0, from Linde) at 120 °C for 1 h and then exposed to a flow of CO₂ or NH₃ (from SIAD) for 1 h. After that, the sample was purged with a flow of He (50 ml min⁻¹) for 20 min at 25 °C in order to remove the weakly adsorbed species. TPD was then started, with a heating rate of 10 °C min⁻¹ till 850 °C. The desorbed products were analysed with a TC detector. The desorbed CO₂ or NH₃, expressed as mmol per gram of catalyst, was determined using a calibration curve.

XPS measurements were performed at normal angle emission with a Specs spectrometer, using the Al K α monochromatic radiation ($h\nu = 1486.7 \text{ eV}$) of an X-ray gun, operating with 300 W (12 kV/25 mA) power. A flood gun with an electron acceleration at 1 eV and electron current of 100 μA was used in order to avoid charging effects. The energy

of the photo ejected electrons was measured using a Phoibos 150 analyzer, operating with a pass energy of 30 eV. The XP spectra were fitted using Voigt profiles combined with their primitive functions for inelastic backgrounds.

Catalytic tests

Hydroisomerization of 1-octene (1.5 mL) was studied using 5 mg of pristine and modified GO and (N)G as catalysts. For reference, defective graphene lacking N-doping derived from alginic acid was tested as well. The reactions were performed in batch mode and mechanical stirring in a pressurized autoclave, following the reaction from 1.5 to 4 h. *n*-Heptane (1.5 mL) was used as solvent. The H₂ pressure and reaction temperature were 30 bar and 80 °C, respectively. Hydrogenation of α -methylstyrene over GO and (N)G was carried out for 1.5 or 4 h in a similar batch autoclave under stirring conditions, at 20 bar H₂ pressure and 70 °C, using 10 mg of catalyst, 1.5 mL of α -methylstyrene using as solvent 3 mL of *n*-hexane. At the required time, the reaction mixture was analyzed with a Thermo Electron Trace GC Ultra/Trace DSQ GC-MS apparatus using a TG-5SilMS, 30 m \times 0.25 mm \times 0.25 μ m capillary column adequate for non-polar mixtures. The oven temperature starts at 60 °C for 2 min and, then, increases at 5 °C \times min till 170 °C that was maintained for 5 min. Only positive ions from $m/z = 50\text{--}300$ amu were analyzed. Hydrogenation of α -methylstyrene over the same catalysts has been carried out using 10 mg catalyst, at 20 bar H₂ and 70 °C, for 4 h, taking 1.5 mL substrate.

Theoretical calculations

Density functional theory (DFT) calculations were performed with a real space uniform grids implementation and within a generalized gradient approximation (GGA) for

electron exchange and correlation [37] using the GPAW program package [38]. The projector augmented wave method (PAW) [39] within the frozen core approximation was used to describe the electron core interaction. A slab model was used for graphene sheet with an optimized C-C bond length (1.426 Å) and a 16 Å vacuum layer between sheets. A zig-zag model of graphene ribbons edges was considered to separate two neighboring edges (Figure 3) [40]. All atoms in the unit cell were allowed to relax and the tolerance was set to 0.05 eV/Å. A grid spacing of 0.2 Å was used and (1,2,1) monkhorst-Pack K meshes were employed to sample the Brillouin zone. Spin polarized calculations were performed with a ferromagnetic (FM) phase on both edges. In the presence of edge defects and impurities the magnetic moments are suppressed.

Results and Discussion

Plasma characteristics

The GO and (N)G samples were treated either in the negative light (NL) or in the positive column (PC) plasma regions. The NL regime is obtained at low pressure (0.2 mbar) and is initiated by electrons that leave the cathode region and are accelerated in the electric field until they reach sufficient energy for ionizations and excitations. Visually, the NL appears as a uniform glow that fills almost the entire volume of the reactor. With increasing the applied voltage and, implicitly, the power dissipated in the discharge, the light becomes more intense due to enhanced excitation-deexcitation processes.

With increasing pressure, the electrons collide more frequently with gas molecules and atoms and lose their energy within shorter distance. Consequently, the length of the NL is gradually

reduced, until it concentrates only in the hollow cathode, for pressures above 0.4-0.5 mbar. Having lost most of their energy in collision processes in the NL, the electrons are too slow to excite or ionize the gas, and thus a dark space appears in front of the cathode. The electrons gain energy from the field throughout this dark space and produce the positive column plasma (PC). For pressures below 1.5 mbar the positive column shows striations unless the discharge is operated under very low current. This regime is rather unstable and was not considered useful for materials treatment. Further increase of the pressure above 2 mbar led to an uniform CP, regardless of the discharge current, in the range 0.6-2.2 mA.

Table 1 lists the samples under study, the experimental conditions for plasma treatment (applied voltage, pressure) and the electrical characteristics of the discharge for each sample treatment. In total the study includes ten samples, six plasma-modified GO and two plasma-modified (N)G, plus the parent materials.

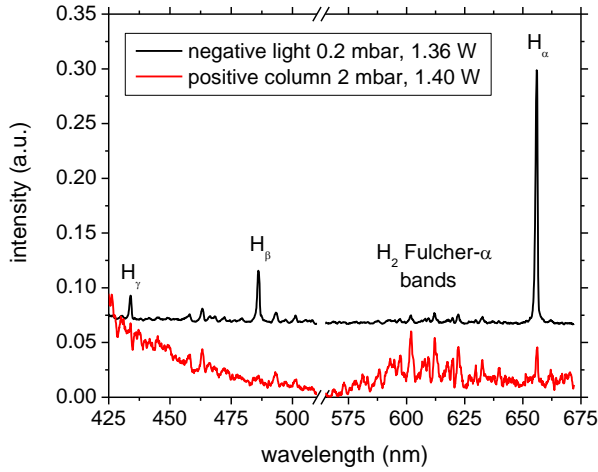
Table 1. Samples under study, experimental conditions for plasma treatment and electrical characteristics of the discharge

Sample ID	Plasma region	Pressure (mbar)	Applied voltage (kV)	Discharge voltage (V)	Discharge current (mA)	Discharge power (W)
GO-NL-2	NL	0.2	2	580	0.71	0.41
(N)G-NL-2						
GO-NL-5	NL	0.2	5	620	2.2	1.36
(N)G-NL-5						

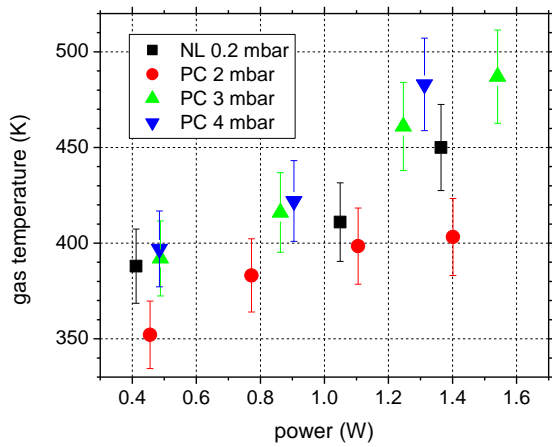
GO-PC-2/2	PC	2	2	680	0.67	0.46
GO-PC-3/2	PC	3	2	800	0.61	0.49
GO-PC-4/2	PC	4	2	850	0.57	0.48
GO-PC-4/5	PC	4	5	800	2.1	1.68

Regarding catalyst modification by plasma, an important parameter is the power dissipated in the discharge (calculated as the current-voltage product). The discharge power increases linearly with applied the voltage, mainly due to the rise in the discharge current. The slope is slightly steeper for higher pressure, resulting in larger power for the PC regime as compared to NL.

Typical emission spectra of the glow discharge in hydrogen are shown in Figure 1(a) for the NL and PC plasma regimes, under similar discharge power.



(a)



(b)

Figure 1. (a) Emission spectra for the H_2 glow discharge operated under the NL regime (0.2 mbar, 1.36 W) and the PC regime (2 mbar, 1.41 W), in the wavelength range 425-675 nm; (b)

The emission in the NL regime is dominated by the atomic hydrogen lines of the Balmer series (H_α - H_γ). The Fulcher- α molecular bands of H_2 have also been identified (590-640 nm), but with much smaller intensity. In the PC regime a low intensity H_α line and a very small H_β line are present, together with a much more intense emission of the Fulcher- α bands and a continuum at wavelengths below 500 nm, also attributed to molecular hydrogen. Thus,

the first obvious difference between the two spectra is the degree of dissociation of molecular hydrogen, which is much larger in the NL than in the PC regime.

From the intensities of the Balmer lines the electron excitation temperature can be determined by the Boltzmann plot method [16]. More details are provided in the SI. For the NL regime, the electron temperature was 8600-9100 K over the investigated power range (0.41-1.36 W). For the PC regime the low intensity of H_{β} does not allow accurate determination of the temperature. However, it is certainly lower than in the NL region.

Another important plasma parameter is the gas temperature, which was determined from the rotational distribution of intensity in the Fulcher- α (2-2)Q band of H_2 . More information on the calculation method is given in the SI. Fig. 1(b) shows the variation of gas temperature as a function of discharge power for NL and CP regimes. The temperature rises with increasing power, the values being in the range 350-490 K for both discharge regimes.

Therefore, the main difference between the NL and PC plasma regions, for similar discharge power, consists in higher H_2 dissociation and higher electron temperature in the NL regime. With rising power, a slight increase of the electron temperature and a more pronounced growth of the gas temperature are observed.

DFT calculations

It has been reported that H_2 plasma may generate atom vacancies on the graphene network [16-18]. Thus, it can be presumed that H_2 plasma treatment of GO and (N)G would generate detachment of O and N atoms. DFT calculations were undertaken to determine the energy needed to remove O or N atoms depending on their coordination to the graphene basal plane and the restructuring of the resulting defects.

To determine the possible effect of H_2 plasma on the detachment of O atoms, calculations were carried out considering the sequential hydrogenation of oxygen from the oxidized graphene nano-ribbons taking as model three alternatives: a) oxygen atom at the edges of GO as C=O groups, b) oxygen as C-O-C ether group between two carbons, and c) O atoms as epoxide between two C atoms. Figure 2 shows the energy diagrams for the removal of each of the three types of O atoms under consideration.

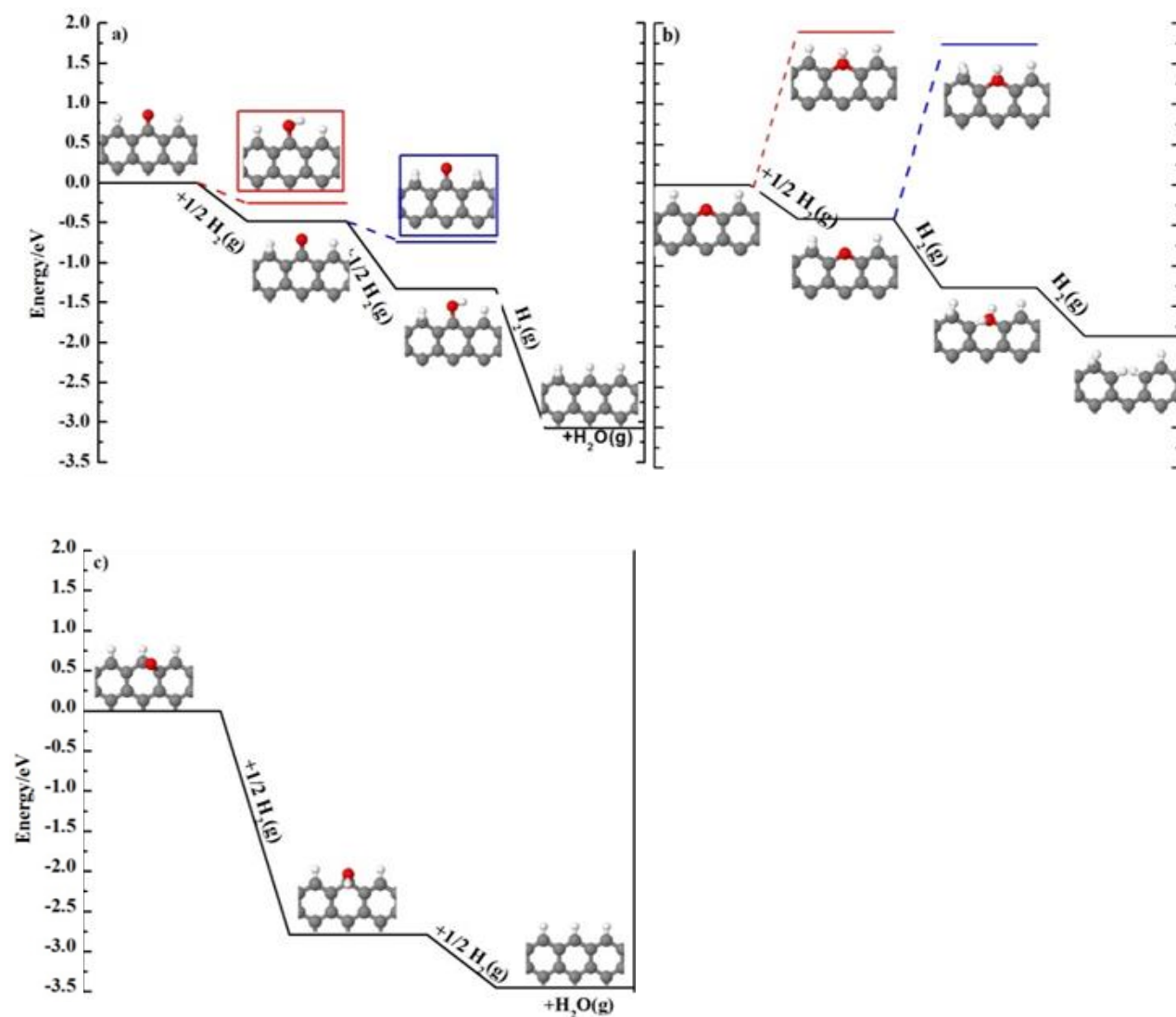


Figure 2. Energy diagram of the O atom removal reaction from graphene models calculated at 0 K for a) O atom at the edges as C=O group, b) O atom inserted between two carbons as C-O-C, and c) O atom as epoxide between two C.

In all three cases, hydrogenation of the O atom is exothermic, resulting in favorable O atom removal. DFT calculations suggest that for the cases of terminal O atom (model a) and O atom in epoxide (model c), O atom removal occurs without any defect formation. However, when O atom corresponds an ether functional group on the graphene lattice, O atom detachment creates a defect that is subsequently involved in a reconstruction process (model b). The exothermicity of O removal in ether groups (model b) is lower than for detachment of terminal or epoxide O atoms and is facilitated by hydrogenation of surrounding C atoms occurring even before the O atom is removed.

Similar calculations were carried out for the detachment of N atoms present in (N)G. In this case the possible influence of the presence of O atoms nearby N atoms, a situation that can occur in (N)G that contains simultaneously both N and O atoms, was also considered. One important issue in the case of N atoms is the preferential detachment of certain types of N atoms that could lead a notable variation in the proportion of the different remaining families of N atoms as consequence of the H₂ plasma treatment with implications in the relative population of catalytic sites.

N atoms inserted in the graphene sheet can occupy different positions, conferring them different properties [19-21]. Thus, the so called “graphitic nitrogen” corresponds to N inset into the graphene plane and bonded to three carbon atoms. In the models, this graphitic

N could be placed far away from the graphene edge or in the vicinity of the edge, the latter exhibiting just a small effect on the activity [22, 23]. Other N sites correspond to pyridinic and pyrrolic atoms on either graphene edges or larger defects. According to literature, the energy associated to these species increases with increasing the distance from the edge. Accordingly, N atoms prefer to substitute carbon atoms near the edge [22, 24]. Based on these preceding calculations, it can be predicted that under plasma conditions promoting the disruption of N atoms from the graphene matrix, the N located at/near the edge would be more prone to detach from the graphene sheet.

Considering these precedents, removal of only graphitic and pyridinic N atoms was considered in the present calculations, since prior characterization by XPS indicates that these two types of families are those present in (N)G. Figure 3 shows the unit cell used as model and the three locations of N on the sheet. Three types of N atoms, pyridinic N (N_p), graphitic N close to the edge (N_{ge}) and graphitic N in the basal plane (N_g), were investigated to determine the energy needed to detach them from graphene. Note that after detachment of N atoms, an atom vacancy will be generated and that this atom vacancy would be the catalytic site to activate molecular hydrogen.

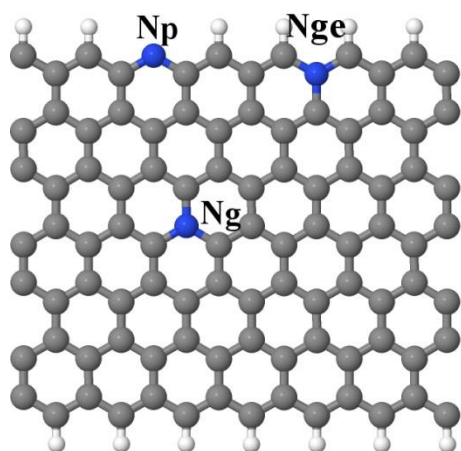
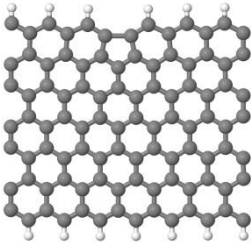
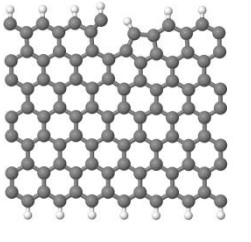
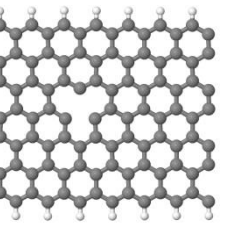


Figure 3. Unit cell of the N-doped graphene model, indicating the location of three types of N considered. N_p : pyridinic, N_{ge} : graphitic near edge, N_g : graphitic in the basal plane.

The energy required to remove any of the three N atom (ΔE_N) considered is indicated in Table 2 together with the top view of the graphene unit cell after the removal of N atom and formation of the atom vacancy. Depending on the location of N, the resulted vacancies have different shapes. These calculations indicate that the endothermic N removal process from the zigzag graphene nanoribbon sheet follows the energy increase order $N_p < N_{ge} < N_g$. Therefore, the removal of the N from the edge (N_p) is expected to be favored during H_2 plasma exposure. Accordingly to data compiled in **Table 2** the energy required to remove the N_g from the basal plane is three times higher than the energy required for N_p at the edge.

Table 2. Energy of removal of N atom placed at various locations in a zig-zag graphene sheet model. Note that removal of N_p atom becomes healed, while removal of N_g generates an atom vacancy on the graphene basal plane.

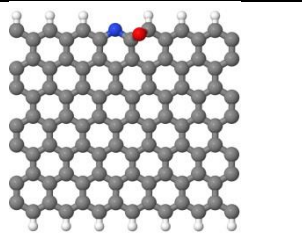
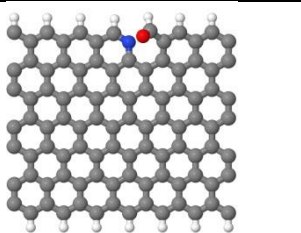
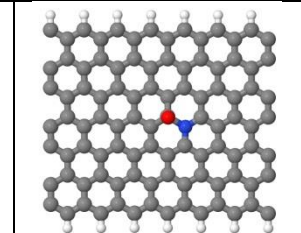
	N_p	N_{ge}	N_g
Top view of reconstituted graphene model after N removal			
ΔE_N (eV)	2.29	4.29	6.85

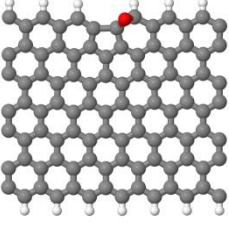
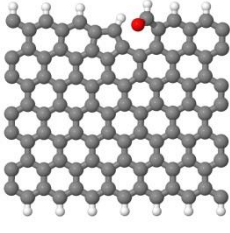
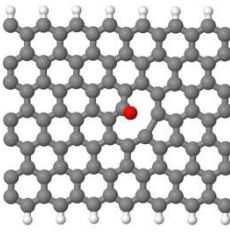
One point to be noted is that no further formation of vacancies takes place after the removal of pyridinic N, but only a reconstruction of the local environment leading to a five

member ring substructure. These vacancies are energetic enough to play a role in the catalytic reaction.

To get understanding concerning the possible contribution of oxidized sites nearby the N center that are likely to be present in (N)G, additional calculations were carried out to evaluate the energy required to remove N atoms in the structures depicted in **Table 3**. These calculations indicate that N removal becomes easier for oxidized surfaces compared to the non-oxidized ones. For the N_{ge} atom, a nearby oxidized carbon favors the disruption of nitrogen only in its pyridinic form, which is more energy demanding than the disruption of N_p . It thus results that irrespective of the nature of the neighbors, the graphitic N atoms are the most difficult to be removed. However, the presence of nearby O atoms changes the geometry of the resulting vacancy compared to the unoxidized structure. These results are also consistent with recent literature reports indicating that the graphitic nitrogen species are more stable than pyrrolic and pyridinic ones, the removal of nitrogen occurring as a multistep process [25].

Table 3. Removal energy of N atoms placed at various locations next to an O-containing carbon site on a zig-zag graphene model. Note that similarly to the models shown in table 2, removal of N_g generates an atom vacancy on the graphene basal plane.

	N_p	N_{ge}	N_g
Graphene nanoribbon			

Top view-oxidized			
Graphene nanoribbon Top view – after N removal			
ΔE_N (eV)	1.28	1.09	3.21

Upon detachment of ether O atoms or N atoms, vacancies are generated. After their formation, these defects can undergo restructuring that would also play a role in catalysis. DFT calculations related to the formation energy of mono- and divacancies in infinite graphene models showed that a $V_2(5-8-5)$ type divacancy is much more stable than a pair of separated mono atomic vacancies ($\approx 7-8$ eV) [26-28]. This result derives from the fact that coalescence of two monovacancies into one divacancy is an exothermic process. Extrapolating, trivacancies have lower energies than separated mono- and divacancy and so on [27, 29]. It is, therefore, concluded from the theoretical study that the formation of large vacancies under plasma irradiation conditions is favored by the low barrier energy of migration of monovacancies (0.9-1 eV) [30]. Previous calculations by DFT at PBE/6-311+G(d,p) level indicate that these monovacancies can activate molecular hydrogen [31].

The GO and (N)G samples under study were also characterized by XRD and spectroscopic techniques (see supporting information, Figures SI.4 and SI.5). Plasma

treatment under the various conditions did not lead to any observable change in XRD, Similarly, no new peaks appeared in the FT-IR spectra of the GO and (N)G samples after plasma treatment under the various conditions, although changes in the relative intensity of the bands could be noted.

This is also the case of Raman spectroscopy, where plasma catalysis treatment increased in general the relative intensity of the D vs. the G band (I_D/I_G) that is a quantitative indicator used to assess the generation of defects. For GO, the I_D/I_G ratio increases in the NL regime with the discharge voltage and in the PC with the voltage and pressure, although NL conditions causes larger I_D/I_G ratios than those of PC. Overall the increase in the I_D/I_G values indicating higher defect density nicely agrees with the enhancement of the catalytic activity (see below), but does not correlate with the power dissipated in the plasma treatment. In the case of (N)G, the I_D/I_G ratio of (N)G-NL-2 did not change respect to the parent (N)G sample and the I_D/I_G increase was apparent only for the (N)G-NL-5. The I_D/I_G for GO samples was lower than those of the (N)G series. Figure S.6 in supporting information collects the Raman spectra of the series of samples and the corresponding I_D/I_G values.

The activity of the samples submitted to plasma treatment as hydroisomerization catalysts is closely related to their ability to adsorb H_2 and with the presence of acid and basic sites. For this reason, information about the changes that plasma treatment produces on H_2 adsorption/desorption and acidity is important. Measurements on temperature-programmed desorption of H_2 , NH_3 and CO_2 revealed that exposure to hydrogen plasma enhances significantly adsorption of these molecules, NL conditions being more effective. These data prove that plasma treatment increases the affinity of GO and (N)G for H_2 , acidity of GO and basicity of (N)G. Chemisorption is also influenced by the nature of the graphene precursor,

GO or (N)G [7]. Thus, (N)G chemisorbs more hydrogen than GO. Plasma treatment of (N)G in the NL at the highest power [(N)G-NL-5] shows a five times enhancement of chemisorbed H₂ as compared to the parent (N)G. The effect of the plasma treatment is even more remarkable for GO, GO-NL-5 exhibits ten times the amount of chemisorbed H₂ than GO, while the CP regime increases H₂ adsorption over three times. H₂-TPD also shows a stronger H₂-chemisorption onto the (N)G than on GO.

H₂ Pulse chemisorption, H₂-TPD, NH₃-TPD and CO₂-TPD

Table 4 presents H₂ Pulse chemisorption, H₂-TPD, NH₃-TPD and CO₂-TPD results for the graphenes exposed to different H₂-plasma conditions compared to the parent ones and reference sample G obtained by pyrolysis of sodium alginate lacking N-doping. Both G and GO showed relatively small chemisorption of hydrogen. Further exposure to hydrogen plasma determines an important enhancement of these up-loaded molecules, LN conditions being more effective. Chemisorption is also influenced by the nature of the graphene precursor, GO or (N)G [7]. Thus, (N)G chemisorbs more hydrogen than GO. According to previous reports, nitrogen atom induces a milder strain in the graphene sheet and as an effect enhances the stability of H chemisorption [32]. That leads to a preferential adsorption of hydrogen on the C atom closest to the defect, with a chemisorption energy that is about twice as large as on pristine graphene.

Plasma treatment of (N)G in the NL at the highest power (LN5) shows a five times enhancement of chemisorbed H₂ as compared to the parent (N)G and four times compared to reduced graphene oxide. The effect of the plasma treatment is even more remarkable for GO: LN5 treatment increases ten times the amount of chemisorbed H₂, while the CP regime over three times. The relative difference between H₂ Pulse chemisorption and H₂-TPD may

account for the capability of graphenes to weakly adsorb hydrogen that is furthermore easily desorbed. However, H₂-TPD also supports a stronger H₂-chemisorption onto the (N)G material than on GO.

NH₃-TPD for GO samples revealed sites corresponding to average strength Lewis and Bronsted acid sites. The acidity of GO has been enhanced by the plasma treatment, and especially by the LN conditions. (N)G exhibited no acidity. However, it showed basic sites of average strength and its exposure to the LN regime enhanced the basicity of these sites. Figure S.7 shows comparative H₂-TPD desorption profiles on the selected samples, confirming a stronger chemisorption on (N)G and the effect of the discharge power.

Table 4. H₂ Pulse chemisorption, H₂-TPD, NH₃-TPD and CO₂-TPD

Solid	H ₂ Pulse chemisorption	H ₂ -TPD			NH ₃ -TPD	CO ₂ -TPD
	mmol/g	Temperature at Maximum °C	mmol/g	Temperature at Maximum (°C)	mmol/g	mmol/g
G	1.26	150	0.32	-	-	-
GO	1.83	179	58.8	>250	0.46	0.04
(N)G	5.32	192	74.8	160–350	0.06	0.15
GO-CP4/2	6.04	204	233.7	> 250	0.58	0
		TOTAL				
GO-CP4/5	6.49	201	247.7	>250	0.74	0
		242	1.5	160–350		
		TOTAL	249.2			
GO-LN2	9.69	200	258.8	>550	1.11	0.02
		326	21.1	160–350		
		TOTAL	279.9			
GO-LN5	17.51	200	289.6	>550	1.26	0
		326	21.0	160–350		
		TOTAL	310.6			
(N)G-LN2	21.24	277	468.5	> 350	0.10	0.27
		381	49.3	180–210		
		TOTAL	517.8			
(N)G-LN5	25.04	184	166.5	> 350	0.09	

	281	606.1	180–210	0.37
	376	60.9		
	TOTAL	833.5		

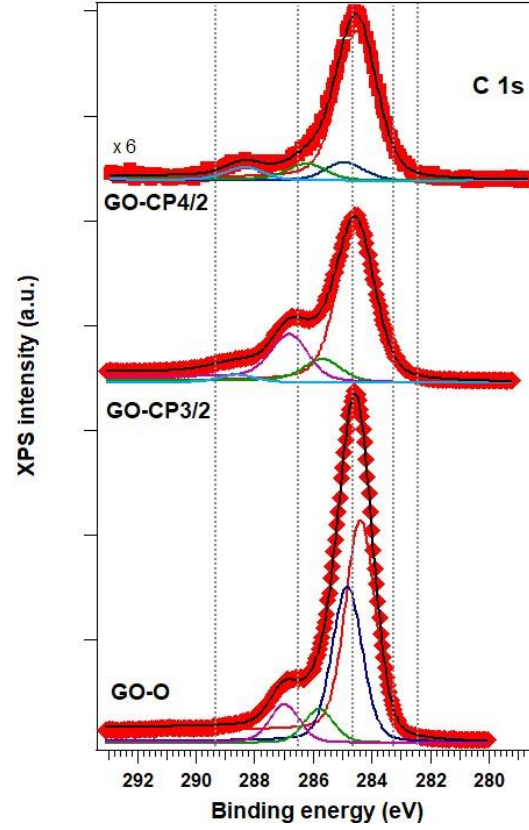
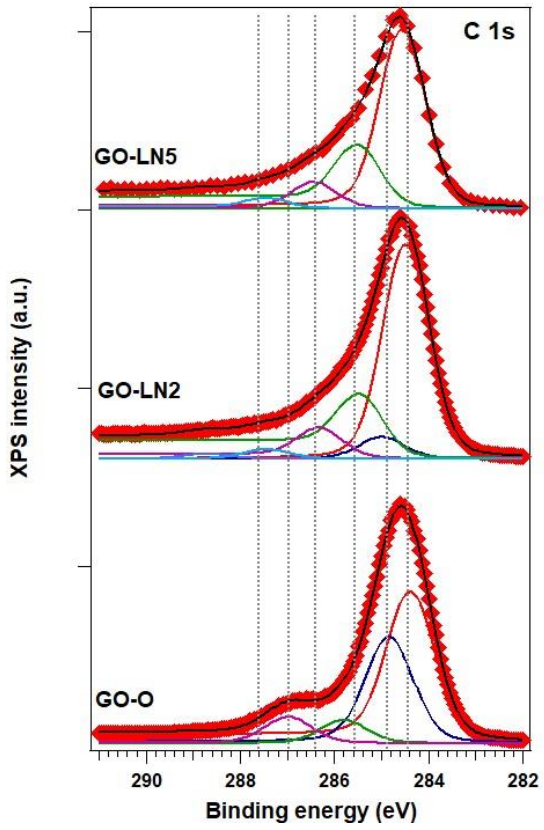
XPS characterization

XPS shows important changes in the components of the peaks corresponding to C, O and N upon plasma treatment, both for GO and (N)G. These changes were significantly larger for the NL discharge regime than for the PC. Figures 3 and 4 provide a detailed description of the evolution of the C, O and N for GO and (N)G as a function of the treatment. The spectrum of the parent GO showed bands attributed to carbon in various surroundings such as C-(C) sp^2 and C-(C) sp^3 at 284.4 and 284.8 eV, and to C-O (287.0 eV) (Figure 3, A). The origins of C1s XPS spectra at 285.5 -286.8 eV for carbon materials is attributed to a charging effect caused by the disconnection of the pathway of electrons between sp^2C and sp^3C specific to graphenes [33, 34]. These are strongly related to the presence of graphene defects such as pentagon, heptagons, and functional groups graphenes [33, 34]. After the exposure to hydrogen in plasma under NL regime, additional bands in the range from 285 to 289 eV accounted on the modification of the parent GO at the level of C-O bonds. The new bands indicate this oxygen transfer occurs with the formation of new C-O and C=O bonds.

Binding energies of the level O1s in these catalysts are depicted in Figure 3, C. They correlated to the information collected from the analysis of the C1s level, corresponding to oxygen in organic C=O (531-532 eV), C-O (532-533 eV) and carbonyl- and ether-type oxygens in ester groups (533.4-535 eV) [35]. A band at around 535 eV has also been observed in other studies dealing with such materials and has been assigned to an overlap with adventitious sodium Auger peak (Na KLL) [36]. The most intense bands for the parent GO

were in the range 532-533 eV. Exposure to hydrogen plasma under the NL regime changed this pattern giving rise to new bands located below 532 eV and around 533.6 eV, respectively, attributed to carbonyl- and ether-type oxygens in ester groups.

The exposure to the CP regime led to different profiles in the XPS spectra. In the energy range associated to the C1s level (Figure 3, B), the dominant deconvolution band shifted to 284.6 eV that might suggest an increased contribution of the C-(C) sp^3 configuration. The bands at 285.5-286.8 eV attributed to the defected graphene [33-34] are still present and with a contribution very close to that in the parent GO, meaning that the aromatic graphene was not much affected by the CP regime. On the contrary, the spectra assigned to the O1s level for these samples showed significant changes in the C-O functionalities of GO (Figure 3 C). For CP3/2 the band at 532.7 eV shifted to 532.2 eV, that at 534.0 eV to 533.4 eV while a new band resulted at 531.0 eV. Further, for CP4/2, the band at 532.7 eV is much less intense as compared to the parent band in the GO, and new bands appeared at 531.5 eV (corresponding to oxygen in organic C=O) [35] and 530.4 eV. The last component might be associated to release oxygen that coordinates on a metallic-like structure, as graphene can also behave [37].



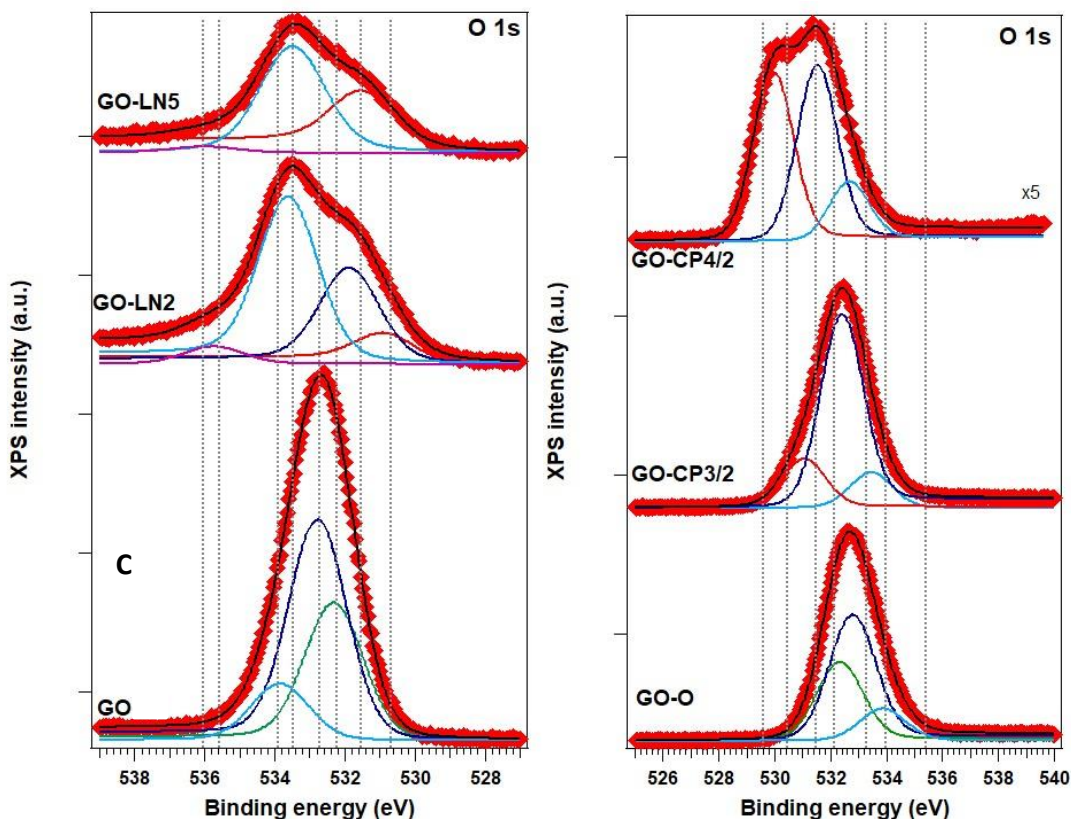


Figure 3. XPS spectra in the regions C1s (A, B) and O1s (C, D) for reference GO and hydrogen plasma treated samples. A and C- LN regime, B and D- CP regime.

Figure 4 show the XPS spectra of fresh and plasma treated (N)G catalysts. The C1s spectrum of the parent G(N) (Figure 4, A) showed bands attributed to carbon in various surroundings such as C-(C) sp^2 and C-(C) sp^3 at 284.4 and 285.2 eV, and residual C-O (287.0 eV) (the XPS O/C ratio: 0.31 for (N)G > 0.13 for (N)G-LN2 > 0.10 for (N)G-LN5). It also presents a component at 286.0 eV attributed to graphene network defects [33-34]. Exposure to plasma under NL regime led to a change in the profile of these spectra: the C-(C) sp^3 band at 284.4 eV shows enhanced intensity as compared to the others, thus suggesting partial removal of nitrogen from the (N)G structure. This is supported by the variation of the XPS N/C ratio: 0.12 for (N)G > 0.05 for (N)G-LN2 > 0.03 for (N)G-LN5, and also by the variation of the XPS N/O ratio: 0.47 for (N)G > 0.39 for (N)G-LN2 > 0.32 for (N)G-LN5.

Changes of the oxygen functionalities are confirmed by binding energies of the level O1s in these catalysts (Figure 4, B). O1s presents components at 531.4 and 533 eV in the spectrum of (N)G, assigned to oxygen in organic C=O and C-O bonds [35]. These bands are not present any more in the spectra of the LN treated samples. Instead, bands at 530.4, 532 and 533.9 eV were evidenced, attributed to oxygen that coordinates on a metallic-like structure, and in carbonyl- and ether-type oxygen in ester groups [35].

Figure 4C shows the XPS spectra of the N1s level. The parent (N)G sample showed bands and 397.4 and 401.0 eV, attributed to C-NH and C=N-C bonds assigned in carbon nitride [38]. After hydrogen plasma exposure these bands shift to 398.3 and 400.5 eV, which is attributed to =N- and -NH- chemical interactions generated by the reduction/disruption of the graphenic carbon-nitrogen bonds [38].

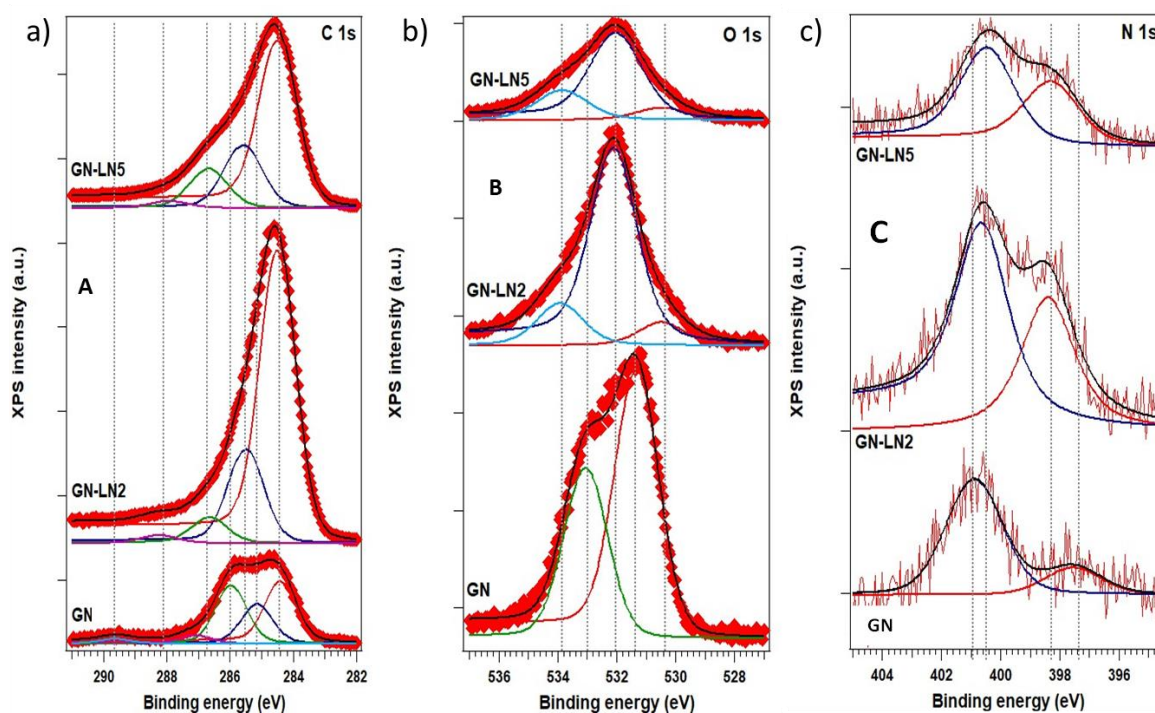


Figure 4. XPS spectra in the regions C1s (a), O1s (b) and N1s (c) for reference (N)G and hydrogen plasma treated (N) samples under LN regime.

An overview of these measurements shows that the C/O atomic ratio of GO increases with the H₂ plasma treatment following the order GO (1.72) < GO-PC-3/2 (3.12) < GO-PC-4/2 (3.70) < GO-NL-2 (6.66) < GO-NL-5 (8.33), indicating the occurrence of O removal, as predicted by DFT calculations. In addition, the relative contribution of the component corresponding to graphitic carbon in the C1s (binding energy 285.4 eV) vs. the total of the C1s peak indicates quantitatively the density of defects. Specifically the components associated to C-O bonds in GO undergo a considerable modification that was larger for the NL conditions than for the PC regime.

In the case of (N)G, plasma treatment also removes residual oxygen and nitrogen atoms as revealed by the increase of the C/O atomic ratio in the order (N)G (3.2) < (N)G-NL-2 (7.69) < (N)G-NL-5 (10.00) as well as the C/N atomic ratio increasing in the same order for (N)G (8.33) < (N)G-NL-2 (20) < (N)G-NL-5 (33.33). As expected in view of the calculations predicting the preferential removal of pyridinic N, notable changes in the N1s peak were observed in the XPS of the (N)G sample after H₂ plasma treatment. Thus, the parent (N)G sample showed N1s bands at 397.4 and 401.0 eV, attributed to pyridinic and graphitic N atoms [32]. After H₂ plasma exposure these bands shift to 398.3 and 400.5 eV, which reflect the changes of the graphene structure [32].

Catalytic behavior of the plasma treated graphenes

Hydroisomerization of 1-octene

Pristine GO and (N)G exhibit similar 1-octene conversion values over the investigated time range (Figure 5), although activation of hydrogen may follow different routes on these materials. The conversion of 1-octene on these catalysts was notably superior to that

measured for the reference G catalyst obtained from sodium alginate lacking N-doping. According to literature, activation of hydrogen can occur in two different types of sites, either frustrated Lewis acid-base pairs and monoatomic carbon vacancies [33]. The first type of sites, requires of heteroatom doping, with centers exhibiting acid and basic properties at a short distance to polarize H₂ molecules. The second type of site appears when there is a carbon (atom) vacancy on the graphene structure and H₂ undergoes dissociation as this molecule approaches the graphene basal plane. DFT calculations at the PBE/6-311+G(d,p) level provides support to monovacancy defects for H₂ activation [31, 34]. The leading hypothesis of the present study is that plasma should enhance the catalytic activity of N-doped graphenes by generation of atom vacancies formed by removal of O or N atoms.

Treatment of GO under the negative glow regime at low power (GO-NL-2) led to an increase of the population of defects, as shown by the Raman data. The created vacancies are able to stabilize H in the form of hydride species, and have as direct effect the increase in 1-octene conversion. For higher power (GO-NL-5) the D/G ratio remained constant, but the conversion continued rising (Figure 5). This is attributed to a further increase in the population of hydroxyls due to the reduction of -C=O and -COOH, as confirmed by XPS measurements. In a very good correlation with the D/G values determined from the Raman experiments, analysis of XPS C1s peak shows that the population of the defects determined from the relative intensity of the 285.5 eV component respect to the total increased from 7.7% for GO to 16.8% for GO-NL-2 and 21.3% for GO-NL-5.

For (N)G, according to literature, direct H₂ dissociation on C-N is less effective [35], but it could be compensated by the presence of defects nearby the N atoms, well reflected through the D/G ratio from the Raman spectra and by analysis of the XPS C1s peak. The

positive influence of defects has been demonstrated for highly ordered carbons such as pyrolytic graphite having little or no activity on the basal plane [36].

According with the positive influence of defects on H₂ activation, plasma treatment of (N)G under NL regime also led to an increase of the conversion (Figure 5). In the case of (N)G, the partial removal of N atoms acting as catalytic sites [35] is compensated by the increase of atom vacancies on the graphene sheet able to stabilize H in the form of hydride species [34]. Accordingly, the relative intensity of the XPS band assigned to the holes in the graphene network, i.e. the band at 285.5 eV, increased from 20.1 % for (N)G to 22.0 % for (N)G-LN2 and 23.0 % for (N)G-LN-5.

The effect of plasma treatment in the PC was only studied for GO. In this case, the performance of GO-PC-2/2 was practically coincident to that of GO, indicating GO is unaffected by H₂ plasma under these conditions, while changing the pressure from 2 to 4 mbar led to a slight increase in the D/G ratio, it remaining constant for GO-PC-4/5 (Figure 6). As an effect of these changes the conversion of 1-octene in the investigated range of time was much smaller compared to that measured for the samples treated under NL regime. Moving from GO-PC-2/2 to GO-PC-4/2 and GO-PC-4/5, respectively, induced only a small increase of the conversion. It is worth to recall that the NL and PC regimes differ with respect to two parameters: the electron energy and the dissociation degree of H₂, which are both larger in the NL.

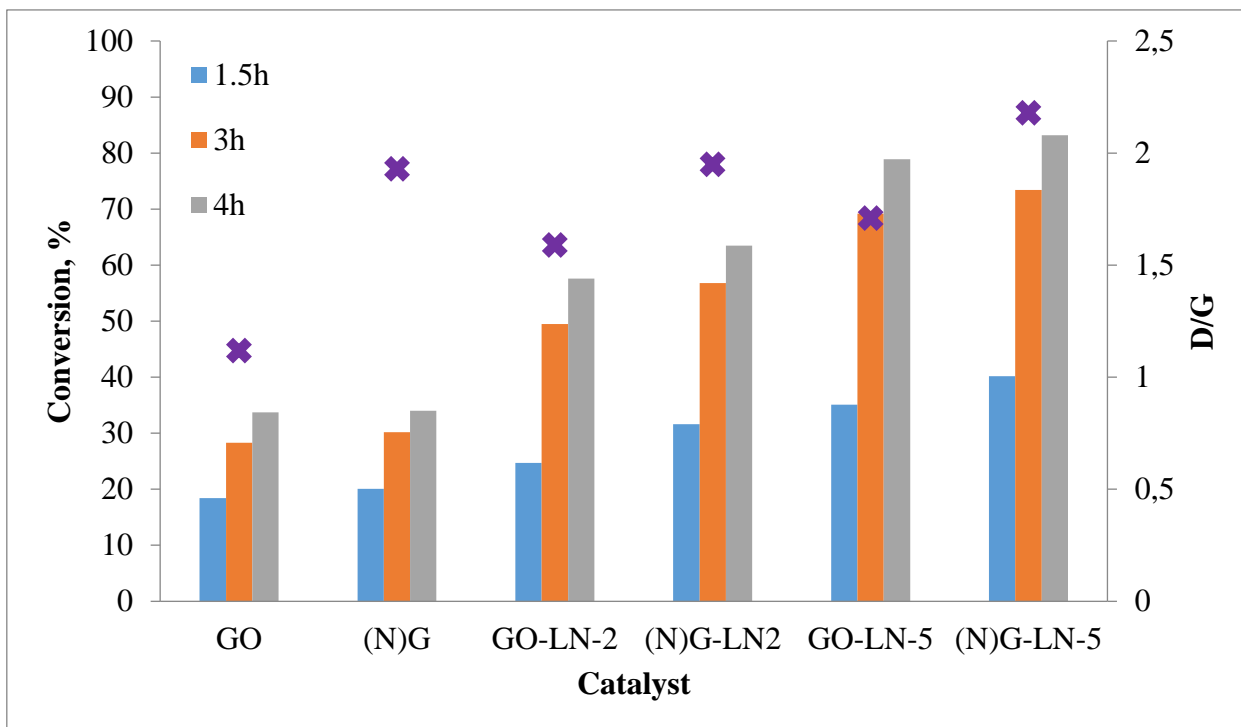


Figure 5. 1-Octene conversion (left axis) over parent GO and (N)G, and over GO and (N)G samples treated by H₂ plasma under negative glow regime at three reaction times in comparison with the relative intensity of the Raman D vs. G bands (right axis, violet crosses). Reaction conditions: 30 bar H₂ pressure, 80 °C, 5 mg of catalyst, 1.5 mL 1-octene and 1.5 mL *n*-heptane as solvent.

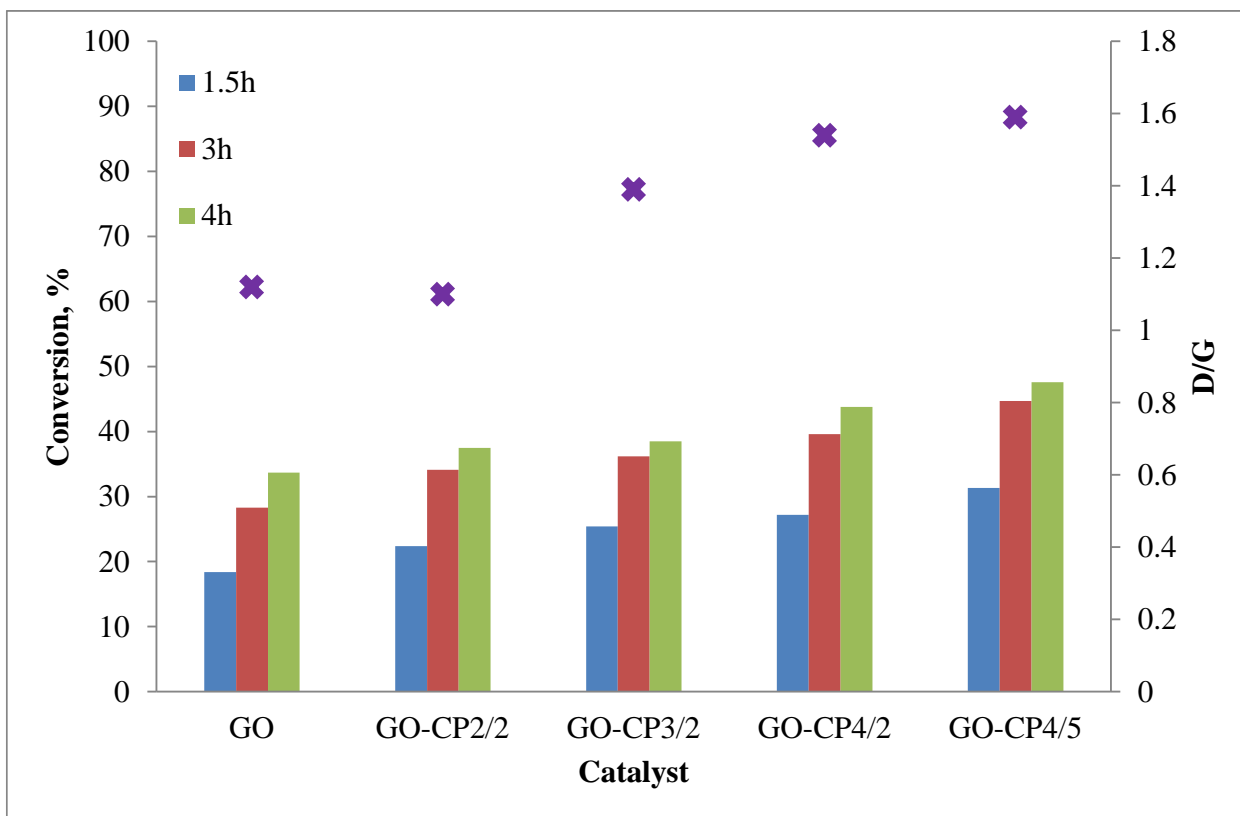
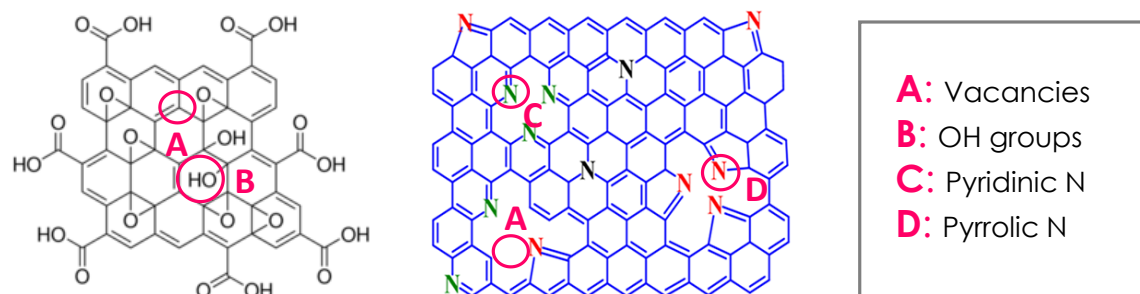


Figure 6. 1-Octene conversion over parent GO and GO treated by H₂ plasma under positive column regime at different reaction times (left axis) in comparison with the intensity of the Raman D vs. G bands (right axis, violet crosses). Reaction conditions: 30 bar H₂ pressure, 80 °C, 5 mg of catalyst, 1.5 mL 1-octene and 1.5 mL *n*-heptane as solvent.

Scheme 1 depicts a proposal of the active sites promoting hydrogenation and isomerization in plasma-treated GO and (N)G. Hydrogenation of 1-octene to octane would occur as a single step process and would be catalyzed by atom vacancies and/or remaining frustrated Lewis acid-base pairs on the GO or (N)G graphenes. The density of the former sites would be enhanced by the treatment with plasma. The isomerization process is more

complex and would occur even as a successive reaction on sites with different acidity/basicity such as hydroxyl and carboxylic groups and pyridinic and pyrrolic N atoms.



Scheme 1. Active sites for hydroisomerization of 1-octene over the investigated GO (left) and (N)G catalysts. Hydrogenation is proposed to occur at carbon vacancies (A), while isomerization would take place at sites B or C and D.

Besides an increase in 1-octene conversion, plasma treatment also promotes skeletal isomerization resulting in the appearance of positional isomers of 1-octene. Figures 7 and 8 show the changes in the selectivity of 1-octene hydroisomerization over pristine GO, (N)G, and H₂ plasma-treated samples for different reaction times. Regardless the catalyst and plasma treatment conditions, the main reaction product was octane. Either a direct pathway, via hydrogenation of 1-alkene, or consecutive reactions, involving firstly isomerization of 1-octene to 2-octene and then the hydrogenation of 2-octene to octane may occur. The possibility of this second indirect route has been proved on these catalysts using 2-octene as substrate, whereby conversion values exceeding 70% with a complete selectivity in octane were observed.

For both GO and (N)G samples, the selectivity to isomerized products was higher for the plasma treated catalysts, no matter the regime of the plasma treatment (Figures 7 and 8).

Considering that plasma treatment increases the acidity and basicity for GO and (N)G, respectively, it is proposed that isomerization of 1-octene to 2-octene is facilitated by the presence of either remnant acid functionalities (GO series) or basic centers associated to nitrogen ((N)G series). The catalytic activity for hydroisomerization parallels the defects induced by the H₂ plasma treatment. The selectivity to octane on the GO-PC series (Figure 7) was higher than those of the GO-NL one, because the acidity of the PC series is weaker, thus, limiting the isomerization reactions.

2-Methyl-1-heptene has also been identified in the reaction products. The acidic and basic centers of plasma treated GO and (N)G will also be responsible for the skeletal isomerization.

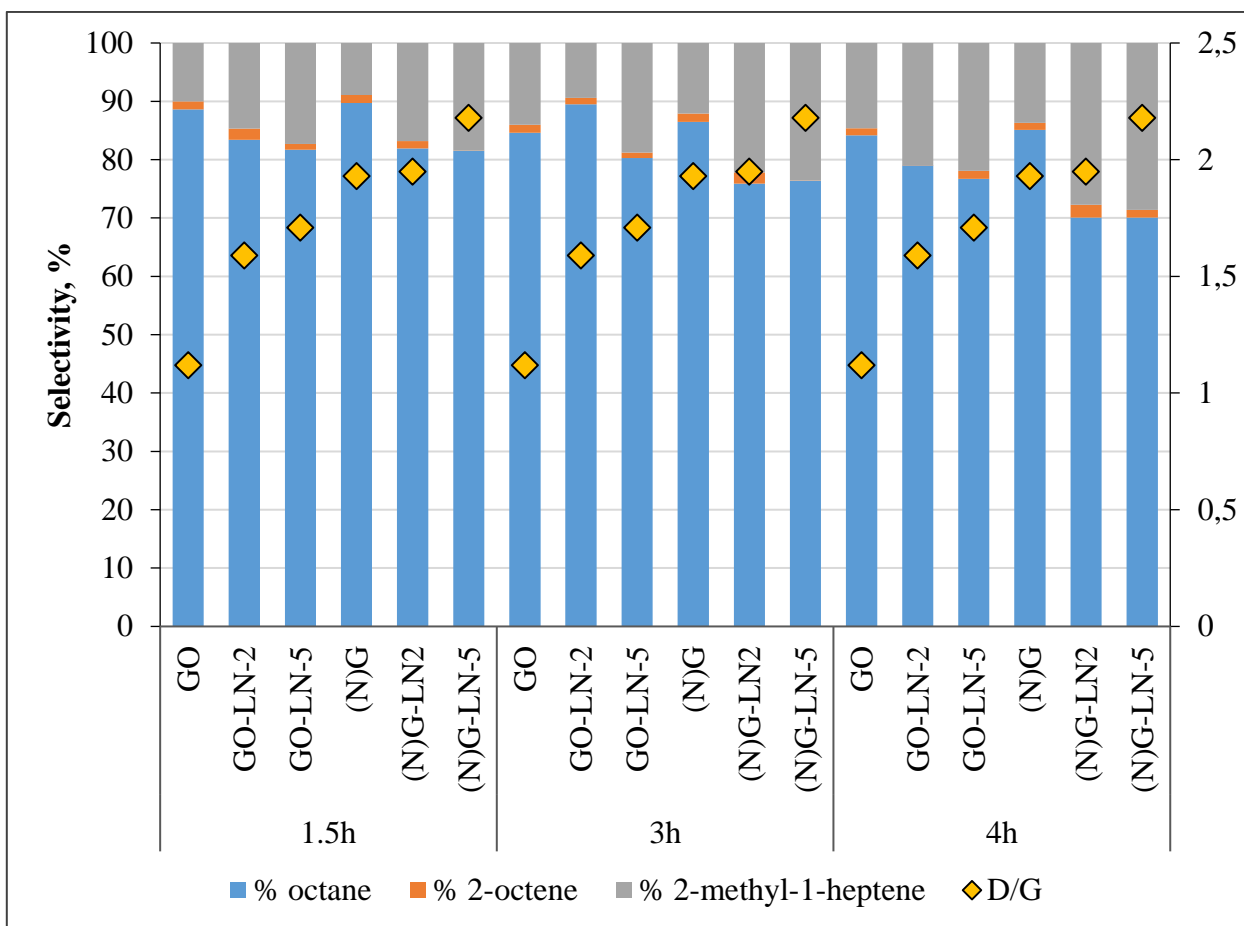


Figure 7. 1-Octene hydroisomerization selectivity (left axis) over the pristine and NL plasma treated GO and (N)G catalysts at 1.5, 3 and 4 h reaction time in comparison with the relative intensity of the Raman D vs. G bands (right axis, orange rombs). Reaction conditions: 30 bar H₂ pressure, 80 °C, 5 mg of catalyst, 1.5 mL 1-octene and 1.5 mL *n*-heptane as solvent.

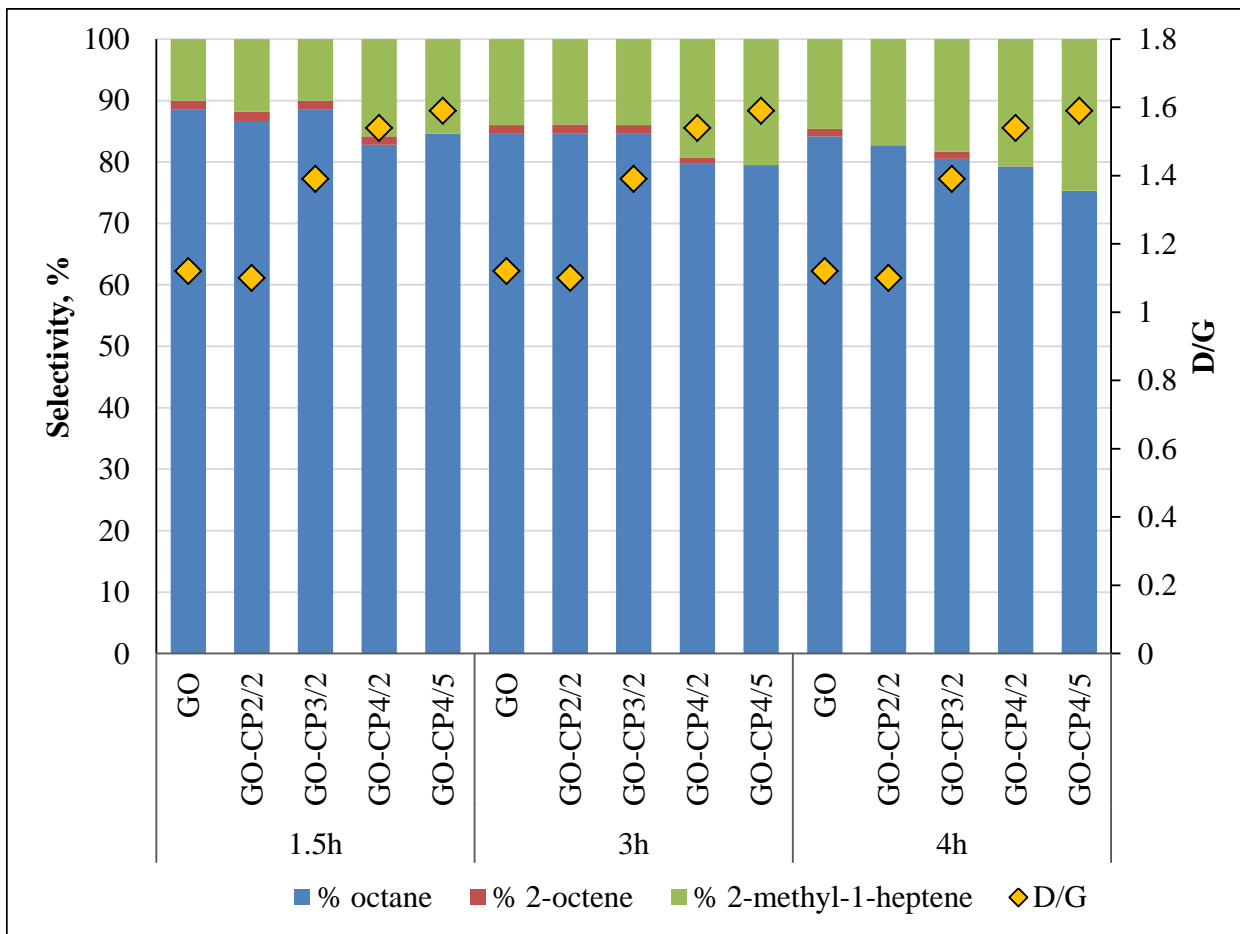


Figure 8. 1-Octene hydroisomerization selectivity (left axis) over pristine and PC plasma treated GO at 1.5, 3 and 4 h reaction time in comparison with the relative intensity of the Raman D and G bands (orange rombs). Reaction conditions: 30 bar H₂ pressure, 80 °C, 5 mg of catalyst, 1.5 mL 1-octene and 1.5 mL *n*-heptane as solvent.

Hydrogenation of α -methylstyrene

Hydrogenation of α -methylstyrene was also investigated on the same catalysts. The reaction occurred only at the double bond with the selective production of *isopropylbenzene* (cumene). The activity of the H₂ plasma activated graphene catalysts followed the same trend

as for the hydrogenation of 1-octene, namely, (N)G led to a slightly higher conversion than GO, and exposure to NL regime enhances more effectively the activity than to PC conditions (Figure 9).

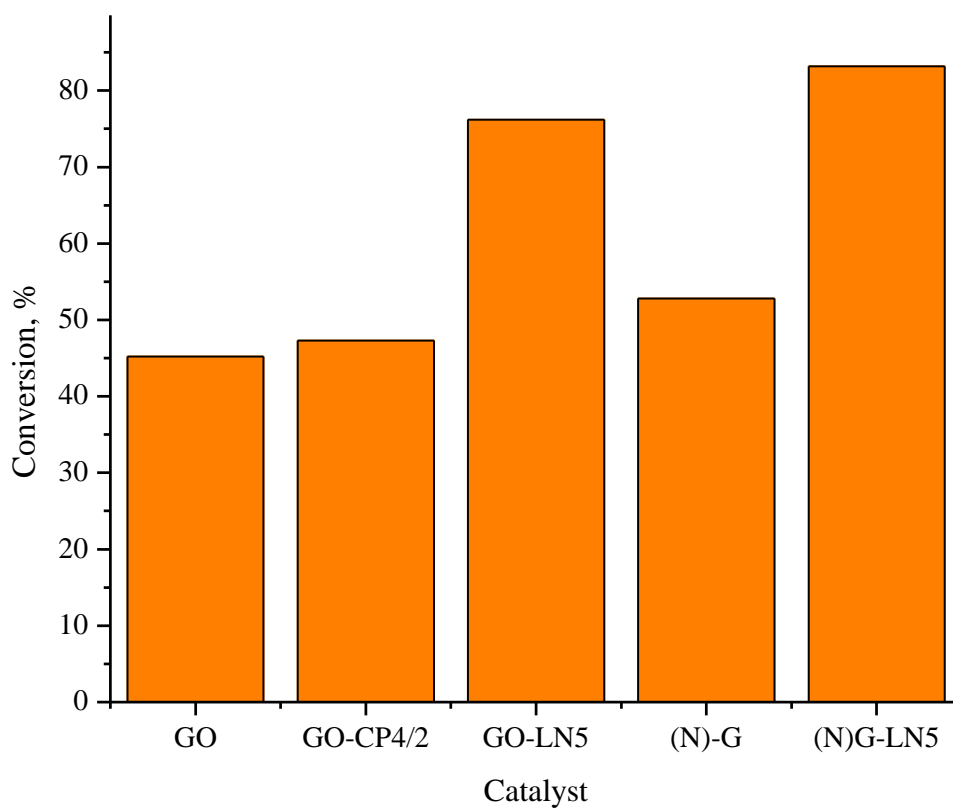
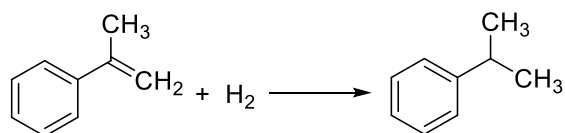


Figure 9. Hydrogenation of α -methylstyrene over pristine and hydrogen plasma modified GO and (N)G. Reaction conditions: 4h, 10 mg catalyst, 70 °C, 20 atm.

Conclusions

The present study illustrates again that plasma can enhance the catalytic activity of GO and (N)G graphenes by increasing atom vacancies derived from the release of O and N atoms. Atom vacancies is one type of graphene defect claimed as active sites to activate molecular hydrogen. But going beyond this existing knowledge, we have provided evidence that the regime of the plasma and the species present plays a key role in the activation of these 2D nanomaterials. Besides the total energy dissipated on the plasma activation process, the conditions of the plasma are crucial to enhance the catalytic activity of graphene and related materials. Thus, samples with a broad range of catalytic activity and selectivity can be obtained by selecting NL conditions in comparison to the PC regime. Catalytic tests using these materials for hydroisomerization of 1-octene and hydrogenation of α -methylstyrene confirms that defects are able to activate both the hydrogenation and isomerization of alkenes. According to the characterization data, the active centers for the hydrogenation generated by plasma are atom vacancies, while isomerization derives from the increase of the acid or basic sites on GO or (N)G, respectively.

Acknowledgements.

This work was supported by the Romanian Ministry of Education and Research UEFISCDI (projects PN-III-P4-ID-PCE-2016-0146, nr. 121/2017, PN-III-P1-1.1-TE-2016-2191, nr. 89/2018 and 16N/2019) and by the Spanish Ministry of Science and Innovation (Severo Ochoa and RTI2018-89237-CO2-R1). MM thanks Dr. F. Gherendi for the calibration of the OES system.

References

- [1] X. Liu, and L. Dai, *Nat. Rev. Materials* 1 (2016) 16064.
- [2] D. Guo, R. Shibuya, C. Akiba, S. Saji, T. Kondo, and J. Nakamura, *Science* 351 (2016) 361-365.
- [3] M.H.M. Ahmed, N. Batalha, H.M.D. Mahmudul, G. Perkins, and M. Konarova, *Bioresour. Technol.* 310 (2020) 123457.
- [4] Y. Lee, S.W. Lee, Y.F. Tsang, Y.T. Kim, and J. Lee, *Chem. Eng. J.* 387 (2020) 124194.
- [5] L.J. Konwar, P. Mäki-Arvela, and J.-P. Mikkola, *Chem. Rev.* 119 (2019) 11576-11630.
- [6] B. Hu, K. Wang, L. Wu, S.H. Yu, M. Antonietti, and M.M. Titirici, *Adv. Mater.* 22 (2010) 813-828.
- [7] A. Primo, F. Neatu, M. Florea, V.I. Parvulescu, and H. Garcia, *Nature Commun.* 5 (2014) 5291.
- [8] A. Dhakshinamoorthy, A. Primo, P. Concepcion, M. Alvaro, and H. Garcia, *Chem. Eur. J.* 19 (2013) 7547-7554.
- [9] M.D. Esrafilii, R. Mohammad-Valipour, S.M. Mousavi-Khoshdeld, and P. Nematollahi, *ChemPhysChem* 16 (2015) 3719-3727.
- [10] C. Rizescu, I. Podolean, J. Albero, V.I. Parvulescu, S.M. Coman, C. Bucur, M. Puche, and H. Garcia, *Green Chem.* 19 (2017) 1999-2005.
- [11] A. Primo, J. He, B. Jurca, B. Cojocar, C. Bucur, V.I. Parvulescu, and H. Garcia, *Appl. Catal. B: Environ.* 245 (2019) 351-359.
- [12] P. Liang, C. Zhang, X. Duan, H. Sun, S. Liu, M.O. Tade, and S. Wang, *Environ. Sci.: Nano* 4 (2017) 315-324.
- [13] X. Chen, W.-D. Oh, P.-H. Zhang, R.D. Webster, and T.-T. Lim, *Chem. Eng. J.* 382 (2020) 122908.
- [14] S.M. Coman, I. Podolean, M. Tudorache, B. Cojocar, V.I. Parvulescu, M. Puche, and H. Garcia, *Chem. Comm.* 53 (2017) 10271-10274.
- [15] N. Ling, Z. Wang, S. Kim, S.H. Oh, J.H. Park, H. Shin, S. Cho, and H. Yang, *ACS Appl Mater Interfaces* 11 (2019) 43460-43465.
- [16] L. Liu, M. Qing, Y. Wang, and S. Chen, *Journal of Materials Science & Technology* 31 (2015) 599-606.
- [17] J.I. Paredes, P. Solís-Fernández, A. Martínez-Alonso, and J.M.D. Tascón, *The Journal of Physical Chemistry C* 113 (2009) 10249-10255.
- [18] R. Rozada, P. Solís-Fernández, J. Paredes, A. Martínez-Alonso, H. Ago, and J. Tascón, *Carbon* 79 (2014) 664-669.
- [19] Z.-H. Sheng, L. Shao, J.-J. Chen, W.-J. Bao, F.B. Wang, and X.-H. Xia, *ACS Nano* 5 (2011) 4350-4358.
- [20] N. Bundaleska, J. Henriques, M. Abrashev, A.M. Botelho do Rego, A.M. Ferraria, A. Almeida, F.M. Dias, E. Valcheva, B. Arnaudov, K.K. Upadhyay, M.F. Montemor, and E. Tatarova, *Sci. Rep.* 8 (2018) 12595.
- [21] R. Yadav, and C.K. Dixit, *J. Sci.: Adv. Mater. Devices* 2 (2017) 141-149.
- [22] M. Li, L. Zhang, X. Quan, J. Niu, and Z. Xia, *J. Catal.* 314 (2014) 66-72.
- [23] J. Quílez-Bermejo, M. Melle-Franco, E. San-Fabián, E. Morallón, and D. Cazorla-Amorós, *J. Mater. Chem. A* 7 (2019) 24239-24250.
- [24] C.K. Lin, *J. Comput. Chem.* 39 (2018) 1387-1397.
- [25] O. Naumov, S. Naumov, B. Abel, and A. Varga, *Nanoscale* 10 (2018) 6724-6733.
- [26] R. Faccio, and A.W. Mombru, *J.Phys.: Condens Matter* 24 (2012) 375304.

- [27] M. Saito, K. Yamashita, and T. Oda, *Jpn. J. Appl. Phys.* 46 (2007) L1185-1187.
- [28] L. Wu, T. Hou, Y. Li, K.s. Chan, and S.T. Lee, *J. Phys. Chem. C* 117 (2013) 17066-17072.
- [29] X.Q. Dai, J.H. Zhao, M.H. Xie, Y.N. Tang, and B. Zhao, *Eur. Phys. J. B* 80 (2011) 343-349.
- [30] J. Paredes, P. Solis-Fernandez, A. Martinez-Alonso, and J.M.D. Tascon, *J. Phys. Chem. C* 113 (2009) 10249-10255.
- [31] G. Sastre, A. Forneli, V. Almasan, V.I. Parvulescu, and H. Garcia, *Applied Catalysis A: General* 547 (2017) 52-59.
- [32] A.P. Dementjev, A. de Graaf, M.C.M. van de Sanden, K.I. Maslakov, A.V. Naumkin, and A.A. Serov, *Diam Relat Mater.* 9 (2000) 1904-1907.
- [33] A. Primo, V. Parvulescu, and H. Garcia, *The journal of physical chemistry letters* 8 (2017) 264-278.
- [34] K. Werner, X. Weng, F. Calaza, M. Sterrer, T. Kropp, J. Paier, J. Sauer, M. Wilde, K. Fukutani, S. Shaikhutdinov, and H.-J. Freund, *J. Am. Chem. Soc.* 139 (2017) 17608-17616.
- [35] X. Chen, D. Deng, X. Pan, Y. Hub, and X. Bao, *Chem. Commun.* 51 (2015) 217-220
- [36] H. Zhou, A. Uysal, D.M. Anjos, Y. Cai, S.H. Overbury, M. Neurock, J.K. McDonough, Y. Gogotsi, and P. Fenter, *Adv. Mater. Interfaces* 2 (2015) 1500277.